Oxidation Kinetics of Hydrogenated Amorphous Carbon (*a*-CH_x) Overcoats for Magnetic Data Storage Media

Yang Yun,[†] Xiaoding Ma,[‡] Jing Gui,[‡] Esteban Broitman,[†] and Andrew J. Gellman*,[†]

Department of Chemical Engineering, Carnegie Mellon University, Pittsburgh, Pennsylvania 15213, and Seagate Technology, Inc., Fremont, California 94538

Received July 19, 2006. In Final Form: January 21, 2007

The oxidation kinetics of *a*-CH_x overcoats during exposure to oxygen and water vapor have been measured using X-ray photoemission spectroscopy (XPS) in an apparatus that allows oxidation and analysis of freshly deposited *a*-CH_x overcoats without prior exposure of the overcoats to air. The uptake of oxygen on the surfaces of the *a*-CH_x overcoats has been measured at O_2 and H_2O pressures in the range $10^{-7}-10^{-3}$ Torr at room temperature. The uptake of oxygen during O_2 exposures on the order of 10^7 Langmuirs leads to saturation of the *a*-CH_x overcoat surfaces at oxidation levels on the order of 20%. This indicates that the surfaces of *a*-CH_x overcoats are relatively inert to oxidation in the sense that the dissociative sticking coefficient of O_2 is $\sim 10^{-6}$. Oxygen uptake during exposure to H_2O vapor is similar to the uptake during exposure to O_2 gas. Although the surfaces of the *a*-CH_x overcoats are quite inhomogeneous, it has been possible to model the uptake of oxygen on their surfaces using a fairly simple Langmuir−Hinshelwood mechanism. Interestingly, the saturation coverage of oxygen during exposure to air at atmospheric pressure is ~6%, significantly lower than that obtained during low-pressure exposure to O_2 gas or H_2O vapor.

1. Introduction

Hydrogenated and nitrogenated amorphous carbon films (*a*-CH_x and *a*-CN_x, respectively) are used to protect the magnetic layer of magnetic data storage hard disks.[1−3] Various types of amorphous carbon have been chosen because of their high hardness, high wear resistance, and chemical inertness. The carbon overcoat provides mechanical protection of the magnetic layer from damage that might occur during contact with the magnetic recording head. It also provides protection of the magnetic layer from oxidation and corrosion by air and humidity. The overcoat itself is, however, subject to oxidation in air and to changes in properties due to oxidation. The oxidation kinetics of the carbon overcoats are the subject of this paper.

The final steps in the production of a magnetic data storage hard disk include the deposition of an *a*-CH_x or *a*-CN_x overcoat film, removal of the disk from the vacuum deposition system in which it is fabricated and the application of the lubricant via dip-coating.[4−6] Removal of the disk from vacuum and exposure to ambient air results in the immediate oxidation of the exposed surface of the *a*-CH_x film, as has been documented by a number of studies using XPS.[7,8] One of the important consequences of the oxidation of the amorphous carbon overcoats is that it influences the adsorption and surface chemistry of the perfluoropolyalkylether (PFPE) lubricants.[9] The interaction of the *a*-CH_x film with the PFPE lubricants can, therefore, be tailored by controlled oxidation of the *a*-CH_x. However, controlled oxidation of the *a*-CH_x requires an understanding of oxygen adsorption on *a*-CH_x overcoats and prediction of the oxidation kinetics.

Many studies of oxygen adsorption on carbonaceous materials have focused on the oxidation of the surfaces of single crystalline materials such as diamond and graphite.[10−21] Among the low Miller index surfaces of natural diamond, the (111) surface exhibits the highest rate of oxidation when exposed to O_2 at temperatures between 900 and 1300 K. The reactivity is lower on the (110) plane and lowest on the (100) plane.[13,15] Arrhenius-

* Corresponding author. E-mail: gellman@cmu.edu. Tel: (412) 268-3848.

[†] Carnegie Mellon University.

[‡] Seagate Technology, Inc.

(1) Casiraghi, C.; Ferrari, A. C.; Ohr, R.; Chu, D.; Robertson, J. Surface properties of ultra-thin tetrahedral amorphous carbon films for magnetic storage technology. *Diamond Relat. Mater.* **2004**, *13* (4−8), 1416.

(2) Ferrari, A. C. Diamond-like carbon for magnetic storage disks. *Surf. Coat. Technol.* **2004**, *180−181*,190.

(3) Hsu, S. M. Nano-lubrication: concept and design. *Tribol. Int.* **2004**, *37* (7), 537.

(4) Gellman, A. J.; Yun, Y. Issues in vapor phase lubrication of magnetic data storage media. *Proc. World Tribol. Cong. 3rd.* **2005**, 63165.

(5) Lei, R. Z.; Gellman, A. J. Humidity effects on PFPE lubricant bonding to a-CHx overcoats. *Langmuir* **2000**, *16* (16), 6628−6635.

(6) Lei, R. Z.; Gellman, A. J. Alkane contamination effects on PFPE lubricant bonding to a-CHx overcoats. *Langmuir*, **2001**, *17* (20), 6240−6247.

(7) Filik, J.; May, P. W.; Pearce, S. R. J.; Wild, R. K.; Hallam, K. R. XPS and laser Raman analysis of hydrogenated amorphous carbon films. *Diamond Relat. Mater.* **2003**, *12*, 974.

(8) Haasz, A. A.; Chiu, S.; Pierre, J. E.; Gudimenko, Y. I. Thermo-oxidative erosion of amorphous hydrogenated carbon films. *J. Vac. Sci. Technol., A* **1996**, *14* (1), 184.

(9) Yun, Y.; Broitman, E.; Gellman, A. J. Adsorption of fluorinated ethers and alcohols on fresh and oxidized carbon overcoats for magnetic data storage. *Langmuir* **2007**, *23*(4), 1953.

(10) Bansal, R. C.; Vastola, F. J. and Walker, P. L., Jr. Kinetics of chemisorption of oxygen on diamond. *Carbon* **1972**, *10* (4), 443.

(11) Barton, S. S.; Harrison, B. H.; Dollimore, J. Surface studies on graphite. Desorption of surface oxides formed on the clean surface at 300K. *J. Phys. Chem.* **1978**, *82* (3), 290.

(12) Curson, N. J.; Wilson, R. J.; Silva, L. A.; Allison, W.; Jones, G. A. C. Studying the kinetics of graphite oxidation using a scanning tunnelling microscope-an undergraduate laboratory experiment. *Eur. J. Phys.* **1999**, *20* (6), 453.

(13) Gozzi, D.; Guzzardi, G.; Salleo, A. High temperature reactivity of different forms of carbon at low oxygen fugacity. *Solid State Ionics* **1996**, *83* (3−4), 177.

(14) Hahn, J. R. Kinetic study of graphite oxidation along two lattice directions. *Carbon* **2005**, *43* (7), 1506.

(15) Jae-Kap, L.; Anderson, M. W.; Gray, F. A.; John, P.; Jin-Yul, L.; Young-Joon, B.; Kwang Young, E. Oxidation of CVD diamond powders. *Diamond Relat. Mater.* **2004**, *13* (4−8), 1070.

(16) Luo, X.; Jean-Charles, R.; Yu, S. Effect of temperature on graphite oxidation behavior. *Nucl. Eng. Des.* **2004**, *227* (3), 273.

(17) Penner, S. S.; Richards, M. B. Oxidation of nuclear-reactor-grade graphite. *Energy* **1988**, *13* (6), 461.

(18) Rodriguez-Reinoso, F.; Thrower, P. A.; Walker, P. L., Jr. Kinetic studies of the oxidation of highly oriented pyrolytic graphites. *Carbon* **1974**, *12* (1), 63.

(19) Zherdev, F. F.; Komissarov, I. E. On the increase of the oxidation rate of irradiated reactor graphite with decreasing temperature. *J. Nucl. Mater.* **1994**, *209* (1), 47.

(20) Ando, T.; Inoue, S.; Ishii, M.; Kamo, M.; Sato, Y.; Yamada, O.; Nakano, T. Fourier-transform infrared photoacoustic studies of hydrogenated diamond surfaces. *J. Chem. Soc., Faraday Trans.* **1993**, *89* (4), 749.

(21) Matsumoto, S.; Kanda, H.; Sato, Y.; Setaka, N. Thermal desorption spectra of the oxidized surfaces of diamond powders. *Carbon* **1977**, *15* (5), 299.

10.1021/la062104e CCC: $37.00
Published on Web 04/14/2007

type behavior is observed for the temperature dependence of the oxidation rate of polycrystalline thin film diamond.[10,13,15] The activation energies for oxidation of polycrystalline thin film diamond are roughly consistent with values reported for natural diamond.[15] Room-temperature oxygen adsorption on natural diamond and polycrystalline diamond thin films is believed to generate functional groups such as carbonyl, acetyl, carboxylic acid, ether, and carboxylic anhydride.[10,21,22] The reaction between oxygen and graphite occurs very slowly at room temperature. The oxidation is usually assumed to be localized at the edge planes of the crystallites where the graphitic layers terminate with unsaturated bonds.[12,13,16]

Previous studies of the oxidation of *a*-CH_x films have focused on the effects of surface oxidation on their optical and electronic properties.[23] It is known that air or O_2 exposure generates oxidized carbon species such as C−O−C, C−OH, and C═O on the surface of the carbon overcoat, thus changing its surface properties.[7,8] However, little is known about the kinetics and mechanism of oxygen adsorption on *a*-CH_x films because the kinetics are more complicated than on either diamond or graphite. The surfaces of *a*-CH_x films are heterogeneous and are composed of carbon atoms with both sp^2 and sp^3 hybridization and varying degrees of hydrogenation.[24−26] Furthermore, the oxidation of freshly sputter deposited *a*-CH_x is so rapid in atmospheric pressure air that the oxidation kinetics have not been studied carefully.

The work described in this paper develops an understanding of the oxidation of freshly deposited *a*-CH_x surfaces. This represents the first such study of the kinetics of *a*-CH_x oxidation using fresh *a*-CH_x surfaces that have never been exposed to air. The deposition of fresh *a*-CH_x films, their oxidation by exposure to O_2 and H_2O, and the measurements of oxygen uptake have all been performed in a single ultrahigh vacuum apparatus. This has allowed precise control of the O_2 and H_2O exposures and elimination of contaminants present in ambient air. The results show that oxidation of the *a*-CH_x surfaces occurs relatively slowly, in the sense that the dissociative sticking coefficient is on the order of 10^{-6}. In spite of the fact that the surfaces of the *a*-CH_x films must be heterogeneous, the oxidation kinetics can be described reasonably well using a simple Langmuir−Hinshelwood model. Finally, we observe that the saturation oxidation level of *a*-CH_x films exposed to air at 760 Torr is lower than the saturation oxidation level reached at oxygen pressures of $<10^{-3}$ Torr.

2. Experimental

All the experiments were performed in an ultrahigh vacuum chamber that allowed the deposition of *a*-CH_x overcoats by magnetron sputtering and exposure of these fresh films to O_2 gas or H_2O vapor at pressures ranging from 10^{-9} to 10^{-3} Torr and temperatures ranging from 80 to 1000 K. Finally, the surfaces of the films were analyzed in situ using XPS to measure the uptake of oxygen on the surface.

The UHV chamber was designed and constructed with the express purpose of studying the vapor-phase lubrication of *a*-CH_x films in situ.[9] The UHV chamber consists of two levels separated by a gate valve. The lower level is used for *a*-CH_x deposition and is pumped with a turbo pump. It is equipped with an Ar^+ ion sputter gun for substrate cleaning, a DC magnetron sputter source (MAK130VCFUHV, 1.3" graphite target, US Inc.) for *a*-CH_x film deposition and one leak valve for introduction of air or O_2 for oxidation of the *a*-CH_x films. In addition, it is equipped with gas flow controllers to allow introduction of a mixture of Ar and CH_4 into the lower level at constant pressure during the sputter deposition process.

The upper level of the UHV chamber is used for surface analysis of films prepared in the lower level and is pumped with a cryo pump and sublimation pump. It is equipped with an X-ray source (XR50, Specs) and a hemispherical electron energy analyzer (CLAM II, VG Scientific), which are used for X-ray photoelectron spectroscopy (XPS). In addition, the upper level is equipped with a quadrupole mass spectrometer (Q200MS, Ametek) for temperature programmed desorption (TPD) studies of $(CF_3CF_2)_2O$ or CF_3CH_2OH adsorbed on the surface of the *a*-CH_x film.

A nickel foil was used as the substrate for deposition of the *a*-CH_x films by magnetron sputtering of a graphite target in the presence of Ar and CH_4. The nickel foil substrate was first cleaned by several cycles of Ar^+ ion sputtering followed by annealing to 950 K before *a*-CH_x film deposition. Films were deposited using a DC power of 75 W at a substrate temperature of 443 K. During the deposition process, the total pressure was maintained at 8 mTorr using a 10% $CH_4/(Ar + CH_4)$ gas mixture. These deposition conditions were identified on the basis of the results of a study of the Raman spectra obtained from films deposited under a variety of different pressures, powers and temperatures. Raman spectroscopy was performed by removing the sample from the UHV chamber and transporting them to Seagate Technology for analysis. The *a*-CH_x film deposition conditions used in this work were chosen to generate *a*-CH_x films which exhibited Raman spectra similar to those of carbon overcoats used commercially. Specifically, these films exhibited Raman spectra with ratios of the D and G peaks and low baseline Raman scattering similar to those of commercial films.[27]

Following deposition of the fresh a-CH_x film, it was exposed to O_2 or H_2O for a controlled period of time within the lower level, vacuum deposition chamber. Exposure of the *a*-CH_x film surface to O_2 or H_2O was conducted by positioning the *a*-CH_x film ∼4 cm from the end of a stainless steel dosing tube that was attached to a vacuum leak valve. An ionization pressure gauge was used to monitor the O_2 or H_2O pressure. All the exposures reported in this work were performed with the sample at 300 K.

Following oxidation, the surface of the film was analyzed using XPS to measure the uptake of oxygen and the evolution of the C 1s feature. All the film deposition, oxidation, and analysis procedures were performed without removing the sample from the UHV chamber. Oxidation of the *a*-CH_x film is readily detectable by monitoring photoelectron emission from the O 1s core level and by the appearance of high binding energy features in the XP spectrum of the C 1s core level. The XP spectra were obtained using a 290 W Mg Kα ($h\nu$ = 1253.6 eV) X-ray source. For high resolution analysis of the spectra, a pass energy of 10 eV was used for the C 1s and O 1s spectra (Figures 1 and 2). For simple measurement of the oxygen uptake, a pass energy of 50 eV was used to increase the signal and decrease the data collection time. The film thickness was determined to be about 70 Å based on the attenuation of the Ni substrate signal. The oxygen content of the oxidized *a*-CH_x film was calculated using the ratio of the integrated areas of the C 1s and O 1s XP spectra. The areas were then scaled by the sensitivity factors of oxygen (0.71) and carbon (0.30) to give

$$\theta_O = \frac{A_O/0.71}{A_O/0.71 + A_C/0.30} \times 100\% \quad (1)$$

where A_O is the integrated area of O 1s XP spectrum and A_C is the area of C 1s XP spectrum.

(22) Kian Ping, L.; Xie, X. N.; Yang, S. W.; Zheng, J. C. Oxygen adsorption on (111)-oriented diamond: a study with ultraviolet photoelectron spectroscopy, temperature-programmed desorption, and periodic density functional theory. *J. Phys. Chem. B* **2002**, *106* (20), 5230.

(23) Godet, C.; Adamopoulos, G.; Kumar, S.; Katsuno, T. Optical and electronic properties of plasma-deposited hydrogenated amorphous carbon nitride and carbon oxide films. *Thin Solid Films* **2005**, *482* (1−2), 24.

(24) Lamperti, A.; Ossi, P. M. Systematic study of amorphous hydrogenated and fluorinated carbon films. *Appl. Surf. Sci.* **2003**, *205* (1−4), 113.

(25) Li Hong, Z.; Hao, G.; Jian Ping, W. Kinetics and mechanisms of laser-induced decompositions of hydrogenated amorphous carbon films on magnetic hard disks. *J. Appl. Phys.* **2002**, *92* (6), 2962.

(26) Gao, G. T.; Mikulski, P. T. Chateauneuf, G. M.; Harrison, J. A. The effects of film structure and surface hydrogen on the properties of amorphous carbon films. *J. Phys. Chem. B* **2003**, *107* (40), 11082.

(27) Marchon, B.; Gui, J.; Grannen, K.; Rauch, G. C.; Ager, J. W.; Silva, S. R. P.; Robertson, J. Photoluminescence and Raman spectroscopy in hydrogenated carbon films. *IEEE Trans. Magn.* **1997**, *33* (5), 3148.

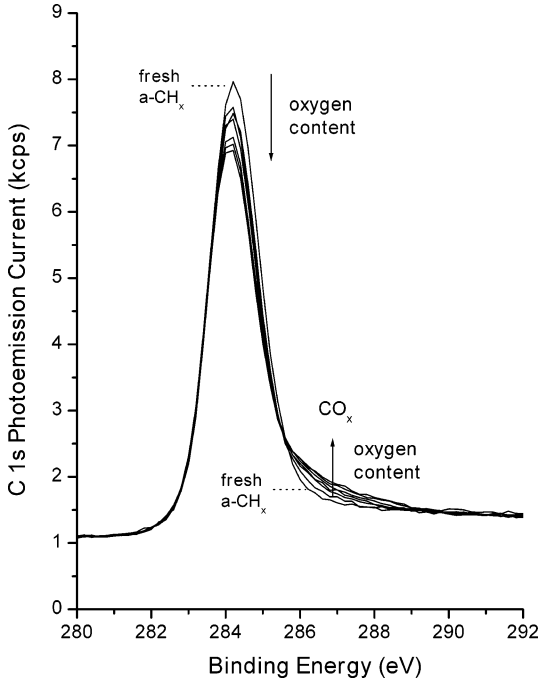

Figure 1. C 1s XP spectra of an O_2-exposed *a*-CH_x film. A fresh *a*-CH_x film was exposed to 1×10^{-4} Torr of O_2 at 300 K. The oxygen content on the film surface increases from 0 to 14%. The shoulder from 285.5 to 289.5 eV grows with increasing oxygen content and is due to CO_x species formed on the surface.

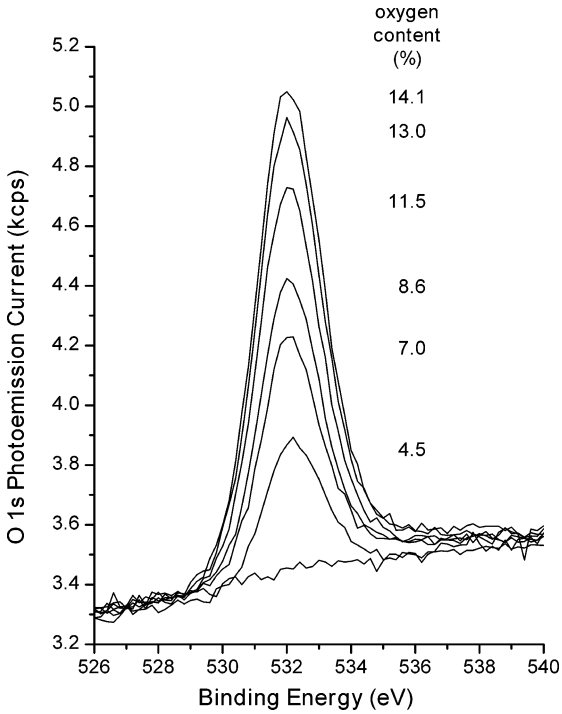

Figure 2. O 1s XP spectra of an O_2-exposed *a*-CH_x film. A fresh *a*-CH_x film was exposed to 1×10^{-4} Torr of O_2 at 300 K. The area under the spectrum is proportional to the oxygen absorbed on the *a*-CH_x surface and has been used to calculate the oxygen content.

3. Results

3.1 *a*-CH_x Oxidation by O_2. Exposure of the fresh *a*-CH_x film to O_2 or air results in the oxidation of its surface. It is known that oxygen will covalently bond to carbon atoms and generate oxidized carbonaceous species such as C−O−C, C−OH, and C═O on the *a*-CH_x surfaces.[7,8] This has been clearly demonstrated using C 1s XP spectra obtained from films exposed to air; however, the oxidation occurs far too rapidly at atmospheric pressure for the oxidation kinetics to be measured. It is only possible to follow the uptake of oxygen with time by using low exposure pressures at which the oxidation occurs over the course of hours.

Oxidation of the fresh *a*-CH_x surfaces has been studied using exposures to O_2 pressures in the range 10^{-7}−10^{-3} Torr for periods of up to 20 h. Figure 1 shows the C 1s XP spectra obtained during exposures to O_2 at pressures of 1×10^{-4} Torr. The ion gauge was used to monitor the O_2 pressure throughout the oxidation process. The *a*-CH_x film was kept at 300 K. Intermittently, the chamber was evacuated to obtain XP spectra of the surface. The C 1s XP spectra in Figure 1 were obtained from an *a*-CH_x film with an oxygen content increasing from 0% to 14%. The fresh *a*-CH_x surface produced immediately after deposition is completely free of oxygen. Attenuation of the C 1s peak at 284.2 eV occurs as a result of both the attenuation of the C 1s signal by adsorbed oxygen and the fact that some of the C 1s signal shifts to higher binding energies. The growth of the shoulder at high binding energy (285.5−289.5 eV) reveals the formation of oxidized carbonaceous species during the exposure to O_2. The C 1s XP spectra obtained during the exposure of the *a*-CH_x film to H_2O vapor are very similar to those observed during exposure to O_2.

The uptake of oxygen on the *a*-CH_x surfaces during exposure to O_2 has been monitored using the XP spectra of the O 1s level. Figure 2 shows the O 1s XP spectra of an *a*-CH_x film obtained during exposure of the surface to 1×10^{-4} Torr of O_2 at 300 K. The shape of the O 1s XPS spectrum is less informative than that of the C 1s level but its intensity can be used to determine the oxygen content of the *a*-CH_x surface. Initially the *a*-CH_x was oxygen free but clearly becomes oxidized over the course of the exposure to O_2. The oxygen content (θ_O) of the *a*-CH_x surface was calculated from the areas under the C 1s and O 1s XP spectra.

The uptake of oxygen, θ_O, on the *a*-CH_x film can be monitored as a function of exposure time to probe the oxidation kinetics. Figure 3 shows the oxygen content as a function of oxidation time at O_2 pressures from 1×10^{-7} to 6×10^{-4} Torr. These data indicate that the rate of oxidation increases with increasing O_2 pressure. All the curves have the appearance of Langmuir uptake curves in that they saturate with high exposure. Multiple repetition of the uptake curve obtained at 2×10^{-4} Torr indicate that the uptake curves are highly reproducible. The absolute O 1s XPS signals are reproducible to ± 5%. In all cases the oxygen content increased monotonically and at the higher pressures appears to reach a saturation value of $\theta_O \approx 20\%$. It seems, however, that the saturation values under different pressures are not exactly the same and are lower at lower pressures. This may be due to limitations on the total exposure times that could be used at low pressures. Saturation requires up to 600 min at an O_2 pressure of 6×10^{-4} Torr. At 10^{-5} Torr the same exposure would require 600 h. Nonetheless, these data provide the most comprehensive picture of *a*-CH_x oxidation kinetics obtained to date.

3.2 Electron Excitation Effects. In order to control the O_2 pressure precisely during oxidation, the ion pressure gauge was kept on throughout the oxidation processes used to collect the data in Figures 1−4. Electrons, ions or excited-state neutrals generated by the ion gauge do seem to have some effect on the oxidation kinetics of the *a*-CH_x film. Figure 4 illustrates this effect. Fresh *a*-CH_x films were exposed to 2×10^{-4} Torr O_2 with the ion gauge either on or off. For the exposures made with the ion gauge off, the gauge was used to determine the pressure as O_2 was being introduced into the chamber but was then turned

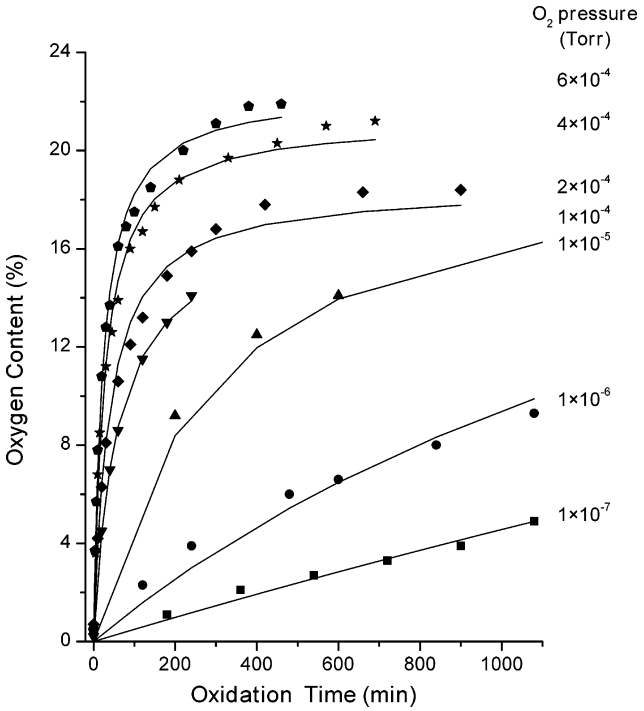

Figure 3. Oxygen content on the *a*-CH_x film surface as a function of oxidation time. The data were measured at O_2 pressures varying from 1×10^{-7} to 6×10^{-4} Torr with the *a*-CH_x film held at 300 K. The solid lines are the fits of a Langmuir adsorption model to the data.

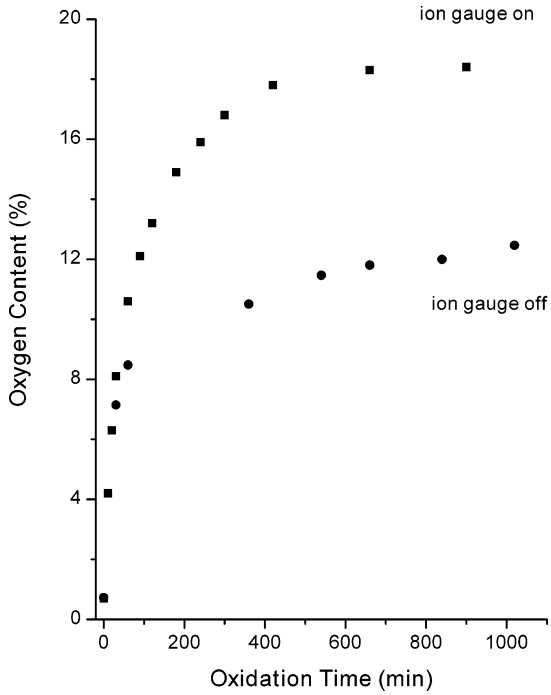

Figure 4. Comparison of oxygen content on *a*-CH_x film surfaces with and without the ion pressure gauge turned on. The data were measured at an O_2 pressure of 2×10^{-4} Torr with the *a*-CH_x film held at 300 K. For the data obtained with the "ion gauge off", the ion pressure gauge was used in the initial 10 min to reach the desired pressure and then was shut off. The ion pressure gauge was turned on for ~30 s every ~30 min during the oxidation to check the O_2 pressure. Species generated by the ion pressure gauge enhance the oxidation of *a*-CH_x films resulting in an increase in the saturation coverage of the oxygen on the surface.

off immediately afterward. The ion gauge was turned on for 30 s every 30 min to check the O_2 pressure and allow correction for drifts in the pressure. It is clear that the ion gauge does have some impact on the oxidation of the *a*-CH_x film. Species created by the ion gauge do not affect the initial uptake of oxygen but do increase the final saturation oxidation level from $\theta_O = 12-18\%$. This suggests that the excited species generated by the ion gauge can react more readily with sites on the *a*-CH_x film surface that are not as readily oxidized by unexcited O_2.

3.3 *a*-CH_x Oxidation by H_2O. During the production of magnetic data storage media, removal of the hard disk from the vacuum deposition chamber results in the exposure of the *a*-CH_x overcoats to air. In addition to contaminants whose concentrations vary from one location to another, ambient air contains water vapor at concentrations as high as 22 Torr (100% RH). Humidity can also cause oxidation of the *a*-CH_x film surface.

The oxidation of *a*-CH_x films by H_2O was investigated using the same procedure as was used for study of oxidation by O_2. Figure 5 shows the oxygen uptake as a function of oxidation time of fresh *a*-CH_x films exposed to 1×10^{-4} Torr H_2O and O_2 at 300 K. The ion pressure gauge was used to monitor the H_2O and O_2 pressure throughout the oxidation process. The ionization gauge sensitivities to O_2 and H_2O are similar (O_2: 1.01, H_2O: 1.12).[28−30] As during the oxidation in O_2, the initial oxygen uptake rate on the surface exposed to H_2O is high but decreases as the oxygen uptake approaches saturation. The XP spectra of *a*-CH_x exposed to H_2O are similar to those of *a*-CH_x exposed to O_2. The only difference is that the oxidation rate is roughly twice as rapid in H_2O as it is in O_2.

3.4 High-Pressure Oxidation of *a*-CH_x. The data in Figure 3 provides a comprehensive view of oxygen uptake on *a*-CH_x overcoats over a broad range of oxygen coverages and at O_2 exposure pressures in the range $10^{-7}-10^{-3}$ Torr. These can be used as the basis for a predictive model of the oxidation kinetics, which ought to be accurate at all pressures provided that there are no processes occurring at very high exposures that are not captured by measurements whose maximum exposure reaches $\sim 10^7$ L (=10 Torr·s). In order to address this issue, we have made a few measurements using exposures at atmospheric pressures. The air-exposed *a*-CH_x was prepared by venting the chamber with one atmosphere of ambient air immediately after film deposition. The *a*-CH_x film was kept in air at room temperature for 1 h, effectively exposing it to 10^{12} L of oxygen. The chamber was then pumped down to 10^{-10} Torr over ~12 h in order to analyze the surface using XPS. Surprisingly, Figure 6 shows that the oxygen coverage is only $\theta_O = 6\%$, significantly lower than the saturation oxygen coverage reached during exposures at low O_2 pressures ($<10^{-3}$ Torr). It is also significantly lower than the total oxygen coverage reached during low-pressure exposures to H_2O vapor. In order to try to eliminate the possible role of air borne contaminants, the *a*-CH_x film was also exposed to 1 atm of clean air (H_2O < 2 ppm, total hydrocarbon <0.1 ppm, CO and CO_2 < 1 ppm) at room temperature for 1 h. The oxygen coverage of the *a*-CH_x exposed to clean air was $\theta_O = 5\%$, still much lower than those at low O_2 pressures.

The observation that the exposure of the *a*-CH_x overcoats to low pressures ($<10^{-3}$ Torr) of O_2 leads to a higher oxygen content

(28) Summers, R. L. *Empirical Observations on the Sensitivity of Hot Cathode Ionization Type Vacuum Gauges*; NASA Technical Report NASA-TN-D-5285; National Aeuronautics and Space Administration: Houston, 1969.

(29) Holanda, R. *Sensitivity of Hot-Cathode Ionization Vacuum Gauges in Several Gases*; NASA Technical Report NASA-TN-D-6815 E-6759; National Aeuronautics and Space Administration: Houston, 1972.

(30) Holanda, R. Investigation of the Sensitivity of Ionization-Type Vacuum Gauges. *J. Vac. Sci. Technol.* **1973**, *10* (6), 1133.

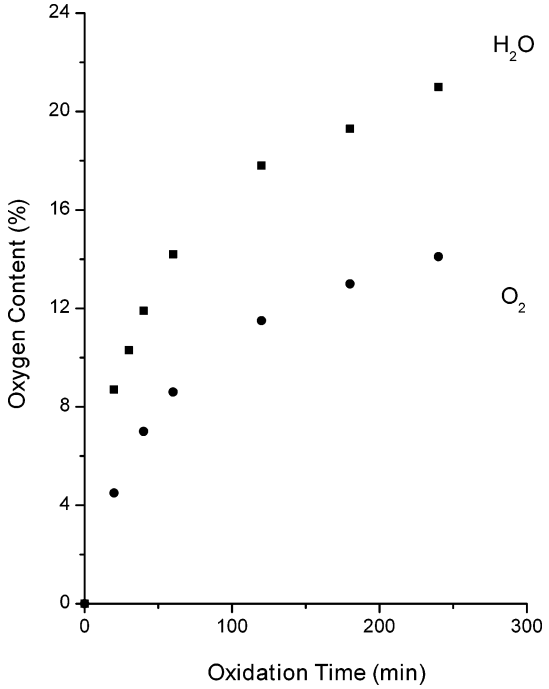

Figure 5. Comparison of oxygen content on *a*-CH$_x$ film surfaces in H_2O vapor and in O_2. The data were measured at 1×10^{-4} Torr with the *a*-CH$_x$ film held at 300 K. The XP spectra of H_2O-exposed *a*-CH$_x$ are qualitatively similar to those of O_2-exposed *a*-CH$_x$. The kinetics of *a*-CH$_x$ oxidation in H_2O are roughly twice as fast as in O_2.

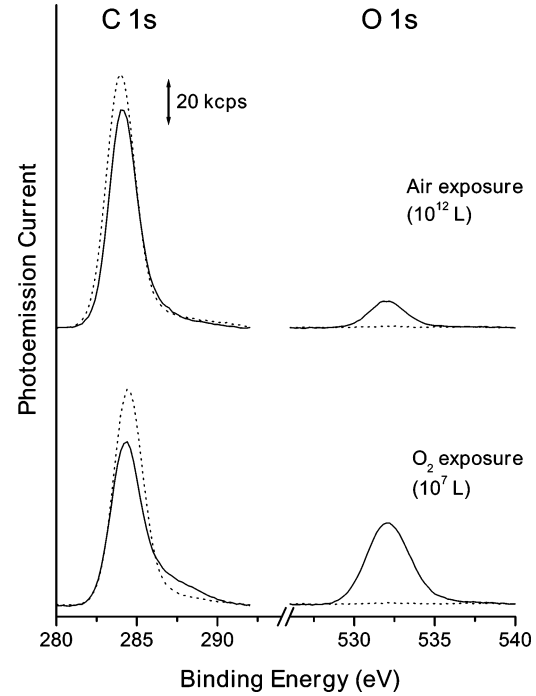

Figure 6. C 1s and O 1s XP spectra of the *a*-CH$_x$ film before (dotted lines) and after (solid lines) exposure to 10^7 L of O_2 (300 K, 10^{-4} Torr) or exposure to 10^{12} L of air (300 K, 760 Torr). The higher exposure to air results in a lower net level of surface oxidation, $\theta_O \approx 6\%$, than the much lower exposure to O_2, $\theta_O \approx 20\%$.

than exposure to high pressures (1 atm) of air is quite interesting and obviously important. It suggests that there must be some very slow oxidation processes that cannot be captured by studies of the oxidation at low pressures ($<10^{-3}$ Torr). These slow oxidation processes must etch the *a*-CH$_x$ overcoats removing the oxygen adsorbed at low exposures in the form of CO or CO_2 and leaving a surface that is inert to further oxidation. Ongoing work is being conducted to test this hypothesis.

4. Discussion

4.1 Oxygen Sticking Coefficient. The dissociative sticking coefficient of O_2 was estimated in order to quantify the reactivity of the *a*-CH$_x$ surface to O_2. The flux of O_2 to the surface at 2×10^{-4} Torr is $F \approx 10^2$ site^{-1}•s^{-1} and yet it takes $\sim 10^4$ s for the oxidation to approach saturation. This indicates that the dissociative sticking coefficient for O_2 is $S \approx 10^{-6}$. It should be noted that because the surface of the *a*-CH$_x$ film is likely to be very heterogeneous, this is a very rough estimate. Locally, the dissociative sticking coefficient might vary by several orders of magnitude between the most and the least reactive sites for oxidation. Nonetheless, this number is much lower than that of reactive metal surfaces, many of which have oxygen sticking coefficients of $S \approx 1$.[31,32] This suggests that there is a significant barrier to the dissociative adsorption of oxygen on the sites exposed by the *a*-CH$_x$ surface. Using the value of $S = 10^{-6}$ one can estimate the time for oxidation of the *a*-CH$_x$ surface at atmospheric pressure and room temperature. The surface of a fresh *a*-CH$_x$ surface is saturated with oxygen within about 10 ms of removal from the vacuum sputter deposition chamber.

4.2 *a*-CH$_x$ Oxidation Kinetics and Mechanism. The oxidation kinetics of the *a*-CH$_x$ films have been modeled using an expression derived from the Langmuir−Hinshelwood mechanism:[33,34]

$$O_{2(g)} \overset{K}{\leftrightarrow} O_{2(ad)} \qquad \theta_{O2} = \theta_{O2}^{sat} \frac{KP_{O2}}{1 + KP_{O2}} \tag{2}$$

$$O_{2(ad)} \overset{k}{\rightarrow} O \qquad r = k\theta_{O2}(\theta_O^{sat} - \theta_O)^2 \tag{3}$$

The first step describes first-order, reversible adsorption of O_2 on empty adsorption sites on the surface with an equilibrium constant *K*. The isotherm relates the equilibrium O_2 coverage (θ_{O2}) to the saturation O_2 coverage (θ_{O2}^{sat}), *K*, and the O_2 pressure (P_{O2}). The molecular adsorption of O_2 is likely to occur via a weak van der Waals interaction with a variety of different sites on the amorphous *a*-CH$_x$ surface. The second step is a second-order irreversible dissociation reaction depositing oxygen onto the surface with a rate constant *k*. The dissociation rate is proportional to *k* and θ_{O2}, and is second-order in the coverage of empty adsorption sites ($\theta_O^{sat} - \theta_O$). Combined and integrated, these two steps yield the oxygen coverage (θ_O) as a function of oxidation time (*t*):

$$\theta_O = \theta_O^{sat} - \left[k\theta_{O2}^{sat} \frac{KP_{O2}}{1 + KP_{O2}} t + (\theta_O^{sat})^{-1} \right]^{-1} \tag{4}$$

The curves in Figure 3 are the fits of this expression to the oxygen coverage measured as a function of oxidation time at seven O_2 pressures. The quality of the fit suggests that the Langmuir model is a reasonable description of the oxidation process. In many respects the quality of the fits is surprisingly good. The Langmuir adsorption model is based on assumptions that the surface is homogeneous and that one can describe O_2 adsorption and dissociation at a given temperature with single

(31) Vesselli, E.; De Rogatis, L.; Baraldi, A.; Comelli, G.; Graziani, M.; Rosei, R. Structural and kinetic effects on a simple catalytic reaction: oxygen reduction on Ni(110). *J. Chem. Phys.* **2005**, *122* (14), 144710.

(32) Vattuone, L.; Burghaus, U.; Savio, L.; Rocca, M.; Costantini, G.; de Mongeot, F. B.; Boragno, C.; Rusponi, S.; Valbusa, U. Oxygen interaction with disordered and nanostructured Ag(001) surfaces. *J. Chem. Phys.* **2001**, *115* (7), 3346.

values of the equilibrium constant, K, and the rate constant, k. Given the complexity of the surfaces of the a-CH_x films, this seems unlikely and yet the fits of eq 4 to the oxygen uptake data are remarkably good. The results show that the Langmuir model can be used to make rough predictions of the oxidation uptake of the a-CH_x overcoats on magnetic data storage hard disks.

The equilibrium constant K for the reversible O_2 adsorption step and the rate constant k for the O_2 dissociation step have been estimated on the basis of the fits of the Langmuir model to the data. The value of K falls in the range 10^3-10^4 $Torr^{-1}$. The value of k is in the range $10^{-8}-10^{-7}$ s^{-1}. At an O_2 pressure of 10^{-4} Torr the values of these constants indicate that the coverage of adsorbed O_2 is roughly $\theta_O \approx 1$ and leads to an adsorption rate consistent with our estimate of 10^{-6} for the dissociative sticking coefficient. This can be understood by viewing the first step as a physisorption process, whereas the second step is a dissociative chemisorption process involving the breaking of oxygen−oxygen bonds and the formation of carbon-oxygen bonds.

5. Conclusions

The oxidation of a-CH_x films is a two step process involving reversible O_2 adsorption followed by dissociation. The net rate constant or dissociative sticking coefficient is $S \approx 10^{-6}$ and indicates that there is a significant barrier to dissociative adsorption. Thus, physisorbed O_2 is much more likely to desorb than dissociate and can equilibrate on the surface in the step prior to dissociation. The uptake of oxygen by exposure of the surface to H_2O occurs with kinetics that are quite similar to those of oxidation by O_2, suggesting a similar process.

Although the surfaces of a-CH_x films are heterogeneous in nature, it appears that the description of their oxidation kinetics in the presence of O_2 is quite simple. Oxidation in O_2 can be described as a Langmuir−Hinshelwood reaction with a relatively low rate constant for oxidation. The values for the adsorption equilibrium constant and the dissociation rate constant obtained in this work can be used as rough estimates for prediction of the oxygen uptake on a-CH_x surfaces under controlled oxidation conditions.

Our results describe the short-term oxidation kinetics of the a-CH_x overcoats during exposures on the order of 10^7 L. At much higher exposures, additional processes reduce the saturation oxidation level of the surface presumably by removal of partially oxidized carbon as CO or CO_2.

Acknowledgment. This work was funded by NSF Grant Number CMS-0408574 and by a grant from the Information Storage Industries Consortium (INSIC).

LA062104E

(33) Strozier, A., Jr.; Cosgrove, G. J.; Fischer, D. A. Oxidation of CO on Pt and Pd. Theory. *Surf. Sci.* **1979**, *82* (2), 481.

(34) Yang, R. T.; Wong, C. Kinetics and mechanism of oxidation of basal plane on graphite. *J. Chem. Phys.* **1981**, *75* (9), 4471−6.